Original Article | Neurointervention

eISSN 2005-8330
https://doi.org/10.3348/kjr.2023.1241
Korean J Radiol 2024;25(6):575-588

Korean Journal of Radiology
KJR

Diagnosis of Unruptured Intracranial Aneurysms Using Proton-Density Magnetic Resonance Angiography: A Comparison With High-Resolution Time-of-Flight Magnetic Resonance Angiography

Pae Sun Suh[1], Seung Chai Jung[2], Hye Hyeon Moon[2], Yun Hwa Roh[3], Yunsun Song[2], Minjae Kim[2], Jungbok Lee[4], Keum Mi Choi[2]

[1]Department of Radiology, Research Institute of Radiological Science and Center for Clinical Imaging Data Science, Yonsei University College of Medicine, Seoul, Republic of Korea
[2]Department of Radiology and Research Institute of Radiology, University of Ulsan College of Medicine, Asan Medical Center, Seoul, Republic of Korea
[3]Department of Radiology, Samsung Medical Center, Sungkyunkwan University School of Medicine, Seoul, Republic of Korea
[4]Department of Clinical Epidemiology and Biostatistics, University of Ulsan College of Medicine, Asan Medical Center, Seoul, Republic of Korea

Objective: Differentiating intracranial aneurysms from normal variants using CT angiography (CTA) or MR angiography (MRA) poses significant challenges. This study aimed to evaluate the efficacy of proton-density MRA (PD-MRA) compared to high-resolution time-of-flight MRA (HR-MRA) in diagnosing aneurysms among patients with indeterminate findings on conventional CTA or MRA.

Materials and Methods: In this retrospective analysis, we included patients who underwent both PD-MRA and HR-MRA from August 2020 to July 2022 to assess lesions deemed indeterminate on prior conventional CTA or MRA examinations. Three experienced neuroradiologists independently reviewed the lesions using HR-MRA and PD-MRA with reconstructed voxel sizes of 0.25^3 mm^3 or 0.2^3 mm^3, respectively. A neurointerventionist established the gold standard with digital subtraction angiography. We compared the performance of HR-MRA, PD-MRA (0.25^3-mm^3 voxel), and PD-MRA (0.2^3-mm^3 voxel) in diagnosing aneurysms, both per lesion and per patient. The Fleiss kappa statistic was used to calculate inter-reader agreement.

Results: The study involved 109 patients (average age 57.4 ± 11.0 years; male:female ratio, 11:98) with 141 indeterminate lesions. Of these, 78 lesions (55.3%) in 69 patients were confirmed as aneurysms by the reference standard. PD-MRA (0.25^3-mm^3 voxel) exhibited significantly higher per-lesion diagnostic performance compared to HR-MRA across all three readers: sensitivity ranged from 87.2%–91.0% versus 66.7%–70.5%; specificity from 93.7%–96.8% versus 58.7%–68.3%; and accuracy from 90.8%–92.9% versus 63.8%–69.5% ($P \leq 0.003$). Furthermore, PD-MRA (0.25^3-mm^3 voxel) demonstrated significantly superior per-patient specificity and accuracy compared to HR-MRA across all evaluators ($P \leq 0.013$). The diagnostic accuracy of PD-MRA (0.2^3-mm^3 voxel) surpassed that of HR-MRA and was comparable to PD-MRA (0.25^3-mm^3 voxel). The kappa values for inter-reader agreements were significantly higher in PD-MRA (0.820–0.938) than in HR-MRA (0.447–0.510).

Conclusion: PD-MRA outperformed HR-MRA in diagnostic accuracy and demonstrated almost perfect inter-reader consistency in identifying intracranial aneurysms among patients with lesions initially indeterminate on CTA or MRA.

Keywords: Brain; Intracranial aneurysm; Magnetic resonance angiography

Received: December 13, 2023 **Revised:** March 8, 2024 **Accepted:** April 3, 2024

Corresponding author: Seung Chai Jung, MD, PhD, Department of Radiology and Research Institute of Radiology, University of Ulsan College of Medicine, Asan Medical Center, 88 Olympicro-43-gil, Songpa-gu, Seoul 05505, Republic of Korea
• E-mail: dynamics79@gmail.com

INTRODUCTION

Unruptured intracranial aneurysms are detected in 0.2%–9% of the general population, according to studies [1,2]. With advances in imaging techniques, the number of intracranial aneurysms diagnosed has increased [2,3]. However, distinguishing unruptured intracranial aneurysms from normal variants, including infundibula, is sometimes challenging, especially small-sized [4,5] and indeterminate lesions, which have been reported in up to 18% of cases using time-of-flight MR angiography (TOF-MRA) on 3T machines [6]. The presence of untreated and unruptured intracranial aneurysms can lead to fear and anxiety, negatively impacting quality of life. Consequently, there is a significant need for accurate diagnosis [7-9]. Digital subtraction angiography (DSA) remains the gold standard for diagnosing intracranial aneurysms, yet it carries risks, including neurological complications, radiation exposure, and the necessity for iodinated contrast media [10]. TOF-MRA, in contrast, is a noninvasive technique that avoids radiation and contrast media exposure and is extensively utilized for the screening and diagnosis of unruptured intracranial aneurysms, showing diagnostic performance comparable to that of CTA [11]. However, the diagnostic efficacy of conventional TOF-MRA is limited in complex cases [12]. While 7T MRI offers superior resolution ranging from 0.2–0.4 mm [13-15], only a handful of studies have assessed its diagnostic value for intracranial aneurysms. Furthermore, its clinical use is restricted by a high specific absorption rate, the limited availability of suitable imaging techniques, and low accessibility [6,16-19].

Proton-density MRA (PD-MRA), utilizing a 3T magnet, excels in differentiating intracranial aneurysms from normal anatomical variations, offering superior visualization of minute vascular structures [5,20,21]. It has a high signal-to-noise ratio (SNR) and supports various advanced techniques, including black blood imaging, compressed sensing, parallel imaging, and iterative reconstruction. Kim et al. [21] highlighted the effectiveness of PD-MRA with voxel dimensions of 0.45 x 0.45 x 0.4 mm^3, specifically for visualizing the posterior communicating artery. Meanwhile, Yim et al. [5] reported outstanding diagnostic performance using PD-MRA. However, their study had limitations, such as comparing PD-MRA to conventional TOF-MRA with inconsistent voxel sizes (0.4^3 or 0.5^3 mm^3) and a predominance of straightforward cases.

We hypothesized that PD-MRA would outperform high-resolution TOF-MRA (HR-MRA) with equivalent spatial resolution in diagnosing intracranial aneurysms and accurately identifying features like infundibula, fenestrations or the precise locations of fine branching arteries. Our objective was to assess the diagnostic capabilities of PD-MRA compared to HR-MRA, as well as the combination of both techniques, in patients with indeterminate findings on previous conventional CTA or MRA exams.

MATERIALS AND METHODS

Study Population

This article adheres to the Standards for Reporting Diagnostic Accuracy Studies (STARD) guideline. It details a retrospective study conducted at a single institution, which received approval from the Institutional Review Board with a waiver for informed consent (IRB No. 2022-0513).

Before recruiting participants, we conducted a preliminary analysis with a small cohort of patients (n = 30) who had undergone both PD-MRA and HR-MRA. This was to estimate the required sample size for our study. The initial findings from these 30 patients showed a sensitivity of 93.3% and a specificity of 100% for PD-MRA, while HR-MRA demonstrated a sensitivity of 53.3% and a specificity of 80%. To calculate the sample size, we used PASS 15 Power Analysis and Sample Size Software (NCSS, Kaysville, UT, USA, https://www.ncss.com/software/pass). We determined the larger sample size needed, choosing between a paired sensitivities test (assuming a sensitivity of 90.0% and 55.0%, with a power of 0.8 and an alpha of 0.015) and a paired specificities test (assuming a specificity of 97.0% and 80.0%, with a power of 0.8 and an alpha of 0.035). The calculation indicated that a sample size of 102 (n = 102) would be sufficient.

The inclusion criteria for this study were as follows: 1) patients who underwent both PD-MRA and HR-MRA scans and 2) patients with indeterminate lesions. An indeterminate lesion was defined as one for which there was insufficient radiological evidence to distinguish an intracranial aneurysm from infundibula or other normal variations based on initial conventional CTA or MRA. Characteristics of these indeterminate lesions included vascular bulges with unclear origins of branching arteries (either the dome or neck), suspected fenestrations, or the anterior communicating artery itself depicted incompletely. The exclusion criteria included: 1) patients who did not undergo DSA, 2) a time interval greater than 6 months between the initial PD-MRA (or HR-MRA) and the

https://doi.org/10.3348/kjr.2023.1241

Korean Journal of Radiology
KJR

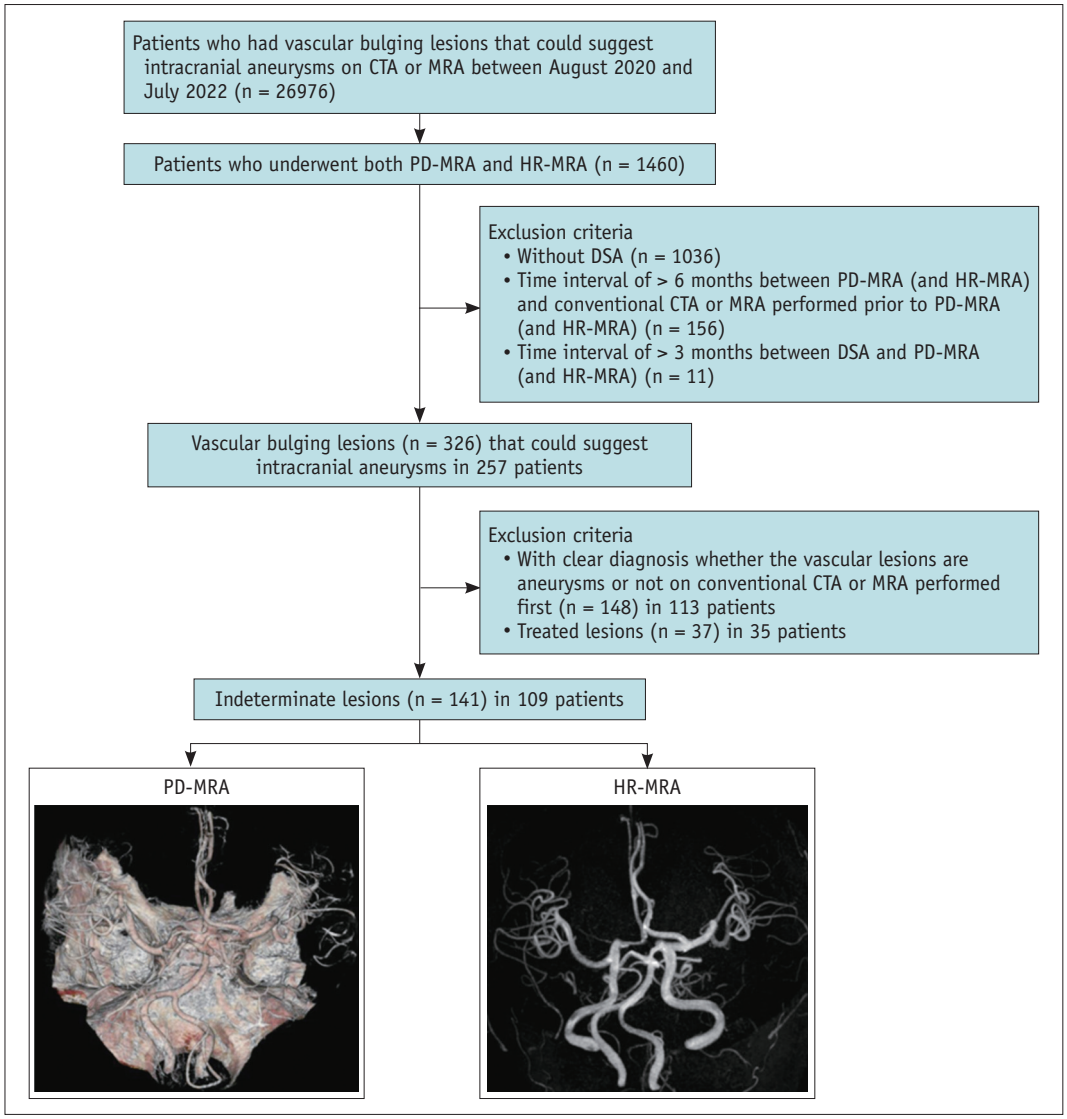

Fig. 1. Flow diagram of patient selection. CTA = CT angiography, MRA = MR angiography, PD-MRA = proton-density MR angiography, HR-MRA = high-resolution time-of-flight MR angiography, DSA = digital subtraction angiography

conventional CTA or MRA, 3) a time interval greater than 3 months between the DSA and the PD-MRA (or HR-MRA), and 4) patients with previously treated lesions (Fig. 1).

Between August 2020 and July 2022, a total of 26976 patients underwent conventional CTA or MRA screenings that revealed potential signs of intracranial aneurysms. These procedures were primarily conducted to assess intracranial artery diseases, such as stenosis, occlusion, or aneurysms, either as part of routine screening in asymptomatic individuals (n = 18344) or in response to symptoms in patients experiencing headaches (n = 5395), dizziness (n = 1888), motor or sensory changes (n = 809), or loss of consciousness (n = 540). Subsequently, PD-MRA and HR-MRA were performed on 1460 patients as part of an advanced imaging protocol following the initial conventional CTA or MRA. These additional scans were aimed at further evaluating the vessels with techniques such as other vessel wall MRIs, with specific indications for the study detailed in the Supplement. The demographics of the patients and the details of the lesions are presented in Table 1.

Image Acquisition

The conventional CTA or MRA scans used for selecting lesions for this study featured spatial resolutions ranging from 0.22 x 0.22 x 0.6 mm^3 to 0.56 x 1.00 x 0.38 mm^3. The specific parameters of these scans are detailed in Supplementary Table 1.

PD-MRA and HR-MRA scans were conducted simultaneously

https://doi.org/10.3348/kjr.2023.1241

Table 1. Patient and lesion details

Patients			
Age, yr		57.4 ± 11.0	
Sex, male:female		11:98	
Symptom			
Asymptomatic		74 (67.8)	
Headache		22 (20.2)	
Dizziness		8 (7.3)	
Motor/sensory change		3 (2.8)	
Loss of consciousness		2 (1.8)	
Conventional imaging performed first			
CTA		11 (9.2)	
MRA		98 (89.9)	
Lesions	Aneurysm	Infundibulum	Others*
Size, mm			
< 3	75 (96.2)	47 (100)	16 (100)
≥ 3	3 (3.8)	0 (0)	0 (0)
Location			
Pcom	17 (21.8)	22 (46.8)	3 (18.8)
ICA	24 (30.8)	4 (8.5)	2 (12.5)
Acom	2 (2.6)	13 (27.7)	3 (18.8)
MCA	10 (12.8)	1 (2.1)	3 (18.8)
ACA	8 (10.3)	4 (8.5)	1 (6.3)
AchA	7 (9.0)	2 (4.3)	3 (18.8)
OphA	4 (5.1)	1 (2.1)	0 (0)
BA	2 (2.6)	0 (0)	1 (6.3)
PCA	2 (2.6)	0 (0)	0 (0)
SCA	2 (2.6)	0 (0)	0 (0)

Data are the number of patients or lesions with the corresponding percentages in parentheses unless specified otherwise. Age is reported as mean ± standard deviation.
*Others included fenestration (n = 4), atherosclerosis (n = 2), and artery itself (n = 10).
CTA = CT angiography, MRA = MR angiography, Pcom = posterior communicating artery, ICA = internal cerebral artery, Acom = anterior communicating artery, MCA = middle cerebral artery, ACA = anterior cerebral artery, AchA = anterior choroidal artery, OphA = ophthalmic artery, BA = basilar artery, PCA = posterior cerebral artery, SCA = superior cerebellar artery

using 3T MR systems (Ingenia CX equipped with a 32-channel head coil, Philips Healthcare, Best, Netherlands), either with or without additional vessel wall MRI techniques. The parameters for the HR-MRA are outlined in Table 2. The PD-MRA with a 0.2^3-mm^3 resolution focused on a smaller scanning field to concentrate on evaluating the circle of Willis.

Image Analysis

The selection of indeterminate lesions from conventional CTA or MRA was carried out by an experienced neuroradiologist (S.C.J.), with 15 years of expertise in neuroradiology.

Three neuroradiologists (S.C.J., with 15 years of neuroradiology experience; P.S.S. and H.H.M., each with 5 years of experience) independently evaluated the indeterminate lesions, classifying them as either aneurysms or non-aneurysms using 0.25^3-mm^3 PD-MRA, 0.2^3-mm^3 PD-MRA, and HR-MRA. They were not informed of the DSA findings and reviewed the images with a two-week wash-out period between assessments of 0.25^3-mm^3 PD-MRA, 0.2^3-mm^3 PD-MRA, and HR-MRA images to minimize recall bias. The image analysis was conducted on a picture archiving and communication system workstation using the AquariusNET viewer version 4.4.13 (TeraRecon, Durham, NC, USA) (Supplementary Fig. 1).

Reference Standard

The reference standard for the final diagnosis was established through a consensus between an experienced neurointerventionist (Y.S.S., with 7 years of experience) and the neuroradiologist (S.C.J., with 15 years of experience in neuroradiology), based on DSA with or without three-

Table 2. Imaging parameters of HR-MRA and PD-MRA

	HR-MRA	0.25^3-mm^3 PD-MRA	0.2^3-mm^3 PD-MRA
Sequence	3D fast field echo	3D turbo spin-echo	3D turbo spin-echo
Repetition time, ms	23	2000	2000
Echo time, ms	3.5	33	35
Flip angle, °	18	90	90
Acceleration mode	Compressed sensing plus SENSE	Compressed sensing plus SENSE	Compressed sensing plus SENSE
Acceleration factor	4	6	4
Matrix	360 x 360 x 140	360 x 360 x 140	452 x 450 x 60
Field of view, mm	180 x 180 x 70	180 x 180 x 70	180 x 180 x 24
Voxel size, mm^3	0.5 x 0.5 x 0.5	0.5 x 0.5 x 0.5	0.4 x 0.4 x 0.4
Reconstructed voxel size, mm^3	0.25 x 0.25 x 0.25	0.25 x 0.25 x 0.25	0.2 x 0.2 x 0.2
Number of excitations	1	1	1
Acquisition time	7 min 32 s	7 min 44 s	6 min 12 s

HR-MRA = high-resolution time-of-flight MR angiography, PD-MRA = proton-density MR angiography, 3D = three-dimensional, SENSE = sensitivity encoding

https://doi.org/10.3348/kjr.2023.1241

Korean Journal of Radiology
KJR

dimensional (3D) rotational angiography (including source images from 3D rotational angiography).

Statistical Analysis

The sensitivity, specificity, and accuracy of diagnosing intracranial aneurysms were calculated by each reader for every imaging modality (HR-MRA alone, PD-MRA alone, and HR-MRA and PD-MRA in combination). We assessed two strategies for integrating HR-MRA and PD-MRA findings: the 'AND' algorithm, indicating an aneurysm only if both modalities identified it as such, and the 'OR' algorithm, indicating an aneurysm if either modality suggested its presence. Diagnostic performance was evaluated on both a per-patient and per-lesion basis. The inter-reader agreement was determined using the Fleiss kappa statistic, where a κ-value < 0.20 signified poor agreement; 0.21–0.40, 0.41–0.60, 0.61–0.80, and 0.81–1 indicated fair, moderate, substantial, and almost perfect agreement, respectively [22]. An experienced statistician (J.B.L., with 19 years of expertise) conducted the statistical analysis using SAS 9.4 (SAS Institute; Cary, NC, USA) and R software version 3.6.1 (R Core Team, Vienna, Austria). A *P*-value < 0.05 was deemed statistically significant. Given the exploratory nature of this study, no adjustments were made for multiple comparisons.

RESULTS

Characteristics of Patients and Lesions

A total of 109 patients (mean ± standard deviation age: 57.4 ± 11.0 years; 98 females) with 141 indeterminate lesions were ultimately included in the study. The majority of these indeterminate lesions (n = 138, 97.9%) measured less than 3 mm in size. Using DSA as the reference standard (DSA alone, n = 10 [9.2%]; and DSA combined with 3D rotational angiography, n = 99 [90.8%]), 78 lesions (55.3%) in 65 patients were identified as aneurysms. The demographics and characteristics of the patients and their lesions are detailed in Table 1.

Diagnostic Performance of PD-MRA and HR-MRA: Per-Lesion Analysis

The diagnostic performance of HR-MRA, PD-MRA, and their combination for diagnosing intracranial aneurysms on a per-lesion basis are shown in Figure 2 and Tables 3 and 4. The sensitivity and specificity of HR-MRA were 66.7%–70.5% (range

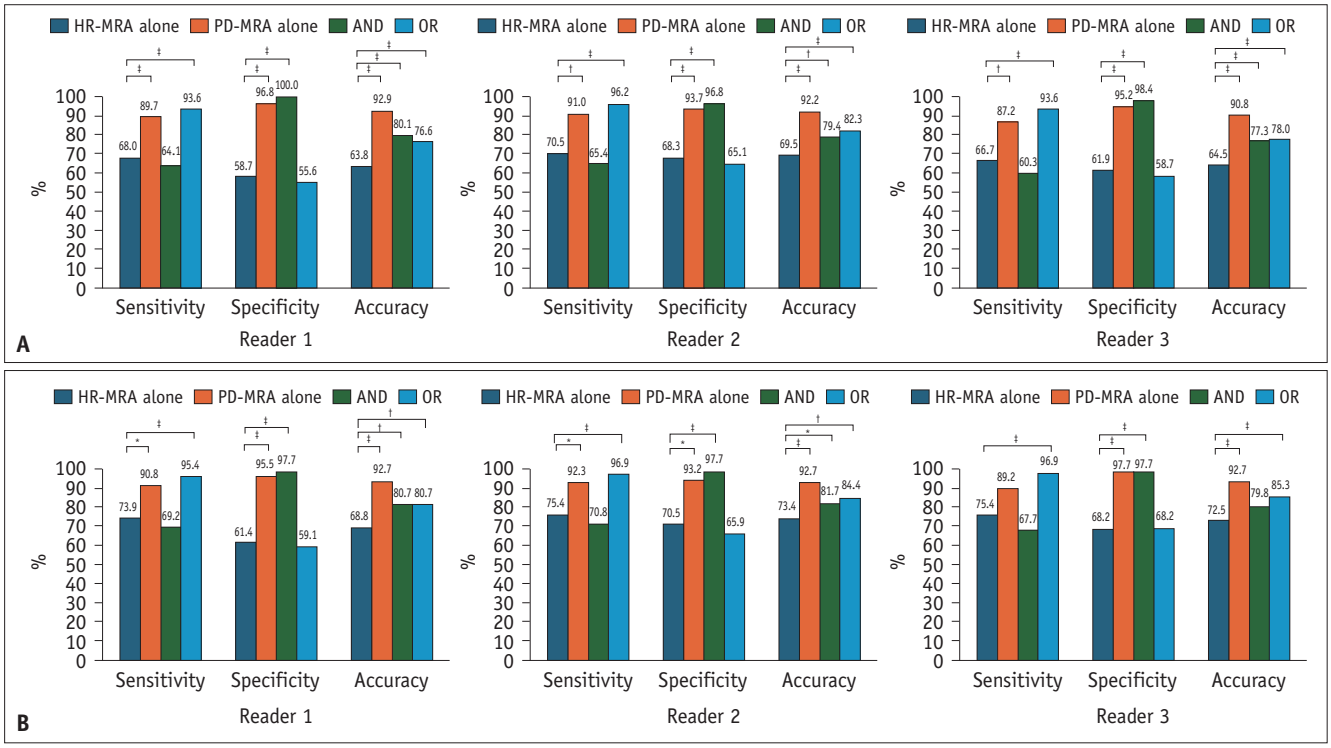

Fig. 2. The diagnostic performance of HR-MRA, 0.25^3-mm^3 PD-MRA, and their combination for diagnosing intracranial aneurysms on a per-lesion **(A)** and per-patient basis **(B)**. **P* < 0.05, †*P* < 0.01, ‡*P* < 0.001. HR-MRA = high-resolution time-of-flight MR angiography, PD-MRA = proton-density MR angiography

https://doi.org/10.3348/kjr.2023.1241

Table 3. Diagnostic performance of HR-MRA, 0.25^3-mm^3 PD-MRA, and its combination on a per-lesion basis

	HR-MRA	0.25^3-mm^3 PD-MRA alone		Combination of HR-MRA and 0.25^3-mm^3 PD-MRA			
				AND		OR	
		Result	*P**	Result	*P**	Result	*P**
Reader 1							
Sensitivity	68.0 (53/78)	89.7 (70/78)	< 0.001	64.1 (50/78)	0.250	93.6 (73/78)	< 0.001
Specificity	58.7 (37/63)	96.8 (61/63)	< 0.001	100 (63/63)	< 0.001	55.6 (35/63)	0.500
Accuracy	63.8 (90/141)	92.9 (131/141)	< 0.001	80.1 (113/141)	< 0.001	76.6 (108/141)	< 0.001
Reader 2							
Sensitivity	70.5 (55/78)	91.0 (71/78)	0.002	65.4 (51/78)	0.125	96.2 (75/78)	< 0.001
Specificity	68.3 (43/63)	93.7 (59/63)	< 0.001	96.8 (61/63)	< 0.001	65.1 (41/63)	0.500
Accuracy	69.5 (98/141)	92.2 (130/141)	< 0.001	79.4 (112/141)	0.004	82.3 (116/141)	< 0.001
Reader 3							
Sensitivity	66.7 (52/78)	87.2 (68/78)	0.003	60.3 (47/78)	0.063	93.6 (73/78)	< 0.001
Specificity	61.9 (39/63)	95.2 (60/63)	< 0.001	98.4 (62/63)	< 0.001	58.7 (37/63)	0.500
Accuracy	64.5 (91/141)	90.8 (128/141)	< 0.001	77.3 (109/141)	< 0.001	78.0 (110/141)	< 0.001

Data are percentages with the number of lesions in parentheses.
**P*-value for the comparison with HR-MRA.
HR-MRA = high-resolution time-of-flight MR angiography, PD-MRA = proton-density MR angiography

Table 4. Diagnostic performance of HR-MRA, 0.2^3-mm^3 PD-MRA, and its combination on a per-lesion basis

	HR-MRA	0.2^3-mm^3 PD-MRA alone		Combination of HR-MRA and 0.2^3-mm^3 PD-MRA			
				AND		OR	
		Result	*P**	Result	*P**	Result	*P**
Reader 1							
Sensitivity	68.0 (53/78)	89.7 (70/78)	< 0.001	64.1 (50/78)	0.250	93.6 (73/78)	< 0.001
Specificity	58.7 (37/63)	96.8 (61/63)	< 0.001	98.4 (62/63)	< 0.001	57.1 (36/63)	1.000
Accuracy	63.8 (90/141)	92.9 (131/141)	< 0.001	79.4 (112/141)	< 0.001	77.3 (109/141)	< 0.001
Reader 2							
Sensitivity	70.5 (55/78)	92.3 (72/78)	< 0.001	66.7 (52/78)	0.250	96.2 (75/78)	< 0.001
Specificity	68.3 (43/63)	95.2 (60/63)	< 0.001	98.4 (62/63)	< 0.001	65.1 (41/63)	0.500
Accuracy	69.5 (98/141)	93.6 (132/141)	< 0.001	80.9 (114/141)	< 0.001	82.3 (116/141)	< 0.001
Reader 3							
Sensitivity	66.7 (52/78)	88.5 (69/78)	0.002	60.3 (47/78)	0.063	94.9 (74/78)	< 0.001
Specificity	61.9 (39/63)	95.2 (60/63)	< 0.001	98.4 (62/63)	< 0.001	58.7 (37/63)	0.500
Accuracy	64.5 (91/141)	91.5 (129/141)	< 0.001	77.3 (109/141)	< 0.001	78.7 (111/141)	< 0.001

Values are percentages with the number of lesions in parentheses.
**P*-value for the comparison with HR-MRA.
HR-MRA = high-resolution time-of-flight MR angiography, PD-MRA = proton-density MR angiography

of all readers, 52–55/78) and 58.7%–68.3% (37–43/63), which were significantly lower than 0.25^3-mm^3 PD-MRA alone (sensitivity: 87.2%–91.0% [68–71/78], $P \leq 0.003$; specificity: 93.7%–96.8% [59–61/63], $P < 0.001$). When using AND combination, the specificity significantly increased (96.8%–100% [61–63/63], $P < 0.001$) compared to HR-MRA, while the sensitivity decreased without statistical significance (60.3%–65.4% [47–51/78], $P = 0.063$–0.250). Conversely, with the OR combination, the sensitivity significantly increased (93.6%–96.2% [73–75/78], $P < 0.001$) while the specificity decreased without statistical significance (55.6%–65.1% [35–41/63], $P = 0.500$). The highest accuracy was achieved with 0.25^3-mm^3 PD-MRA alone (90.8%–92.9% [128–131/141]), which was significantly superior to HR-MRA (63.8%–69.5% [90–98/141], $P < 0.001$). The accuracy of AND and OR combinations was also significantly higher than HR-MRA. Results were similar to that of 0.2^3-mm^3 PD-MRA. Inter-reader agreement between the three readers was moderate ($\kappa = 0.447$) with HR-MRA, while almost perfect with 0.25^3-mm^3 PD-MRA ($\kappa = 0.820$) and 0.2^3-mm^3 PD-MRA ($\kappa = 0.849$). The cross-tabulations of HR-MRA and PD-MRA interpretations for each reader are shown in Table 5. The

https://doi.org/10.3348/kjr.2023.1241

Korean Journal of Radiology
KJR

Table 5. HR-MRA and PD-MRA interpretations in the 141 indeterminate lesions of 109 patients

Reader	0.25^3-mm^3 PD-MRA			0.2^3-mm^3 PD-MRA		
	Aneurysm	Not aneurysm	Total	Aneurysm	Not aneurysm	Total
Reader 1						
HR-MRA						
Aneurysm	50 (46)	29 (19)	79 (65)	51 (46)	28 (19)	79 (65)
Not aneurysm	22 (15)	40 (29)	62 (44)	21 (15)	41 (29)	62 (44)
Total	72 (61)	69 (48)	141 (109)	72 (61)	69 (48)	141 (109)
Reader 2						
HR-MRA						
Aneurysm	53 (47)	22 (15)	75 (62)	53 (48)	22 (14)	75 (62)
Not aneurysm	22 (16)	44 (31)	66 (47)	22 (16)	44 (31)	66 (47)
Total	75 (63)	66 (46)	141 (109)	75 (64)	66 (45)	141 (109)
Reader 3						
HR-MRA						
Aneurysm	48 (45)	28 (18)	76 (63)	48 (45)	28 (17)	76 (63)
Not aneurysm	23 (14)	42 (32)	65 (46)	24 (14)	41 (32)	65 (46)
Total	71 (59)	70 (50)	141 (109)	72 (60)	69 (49)	141 (109)

Data indicate the numbers of lesions, along with the numbers of patients in parentheses.
HR-MRA = high-resolution time-of-flight MR angiography, PD-MRA = proton-density MR angiography

examples of true-positive and true-negative cases correctly identified on PD-MRA are shown in Figures 3 and 4, respectively.

Diagnostic Performance of PD-MRA and HR-MRA: Per-Patient Analysis

The diagnostic performance on a per-patient basis is illustrated in Figure 2 and detailed in Supplementary Tables 2 and 3. For reader 1, the sensitivity of 0.25^3-mm^3 PD-MRA was significantly higher than that of HR-MRA in reader 1 (0.25^3-mm^3 PD-MRA vs. HR-MRA, 90.8% [59/65] vs. 73.9% [48/65]; $P = 0.013$), as it was for reader 2 (92.3% [60/65] vs. 75.4% [49/65]; $P = 0.01$), but this difference was not statistically significant for reader 3 (89.2% [58/65] vs. 75.4% [49/65]; $P = 0.064$). The specificity and accuracy were significantly higher for PD-MRA compared to HR-MRA across all readers ($P < 0.001$–0.013). When the AND combination strategy was used, specificity significantly increased (97.7% [43/44], $P < 0.001$), while sensitivity decreased, though not significantly (67.7%–70.8% [44–46/65], $P = 0.063$–0.500). Conversely, the OR combination strategy significantly increased sensitivity (95.4%–96.9% [62–63/65], $P < 0.001$) but decreased specificity, although not significantly (59.1%–68.2% [26–30/44], $P = 0.500$–1.000). The results were similar for the 0.2^3-mm^3 PD-MRA. Inter-reader agreement among the three readers was moderate ($\kappa = 0.510$) with HR-MRA but almost perfect with both 0.25^3-mm^3 PD-MRA ($\kappa = 0.864$) and 0.2^3-mm^3 PD-MRA ($\kappa = 0.888$).

False-Positive and False-Negative Lesions

Regarding false positive results, an aneurysm in the A1 segment of the right anterior cerebral artery was consistently missed by two or more readers, situated near the brain parenchyma.

In terms of false negative (FN) results, seven aneurysms (paraclinoid internal cerebral artery [ICA], n = 4; middle cerebral artery, n = 2; cavernous ICA, n = 1) were consistently missed by two or more readers, and 2 paraclinoid ICA aneurysms were missed by all readers. Five of these aneurysms were located near the cavernous sinus, sphenoid sinus, or clinoid bones, where susceptibility artifacts or indistinct margins may contribute to the FN outcomes (Fig. 5). Two missed M1 segment lesions were positioned close to the brain parenchyma or tortuous arteries, potentially complicating their interpretation. In one instance of a paraclinoid ICA lesion, PD-MRA identified a branching artery emerging from the dome of the lesion, whereas DSA did not visualize this branching artery, resulting in FN findings (Fig. 6).

DISCUSSION

PD-MRA demonstrated superior diagnostic performance compared to HR-MRA at the same spatial resolution in distinguishing intracranial aneurysms from normal

 https://doi.org/10.3348/kjr.2023.1241

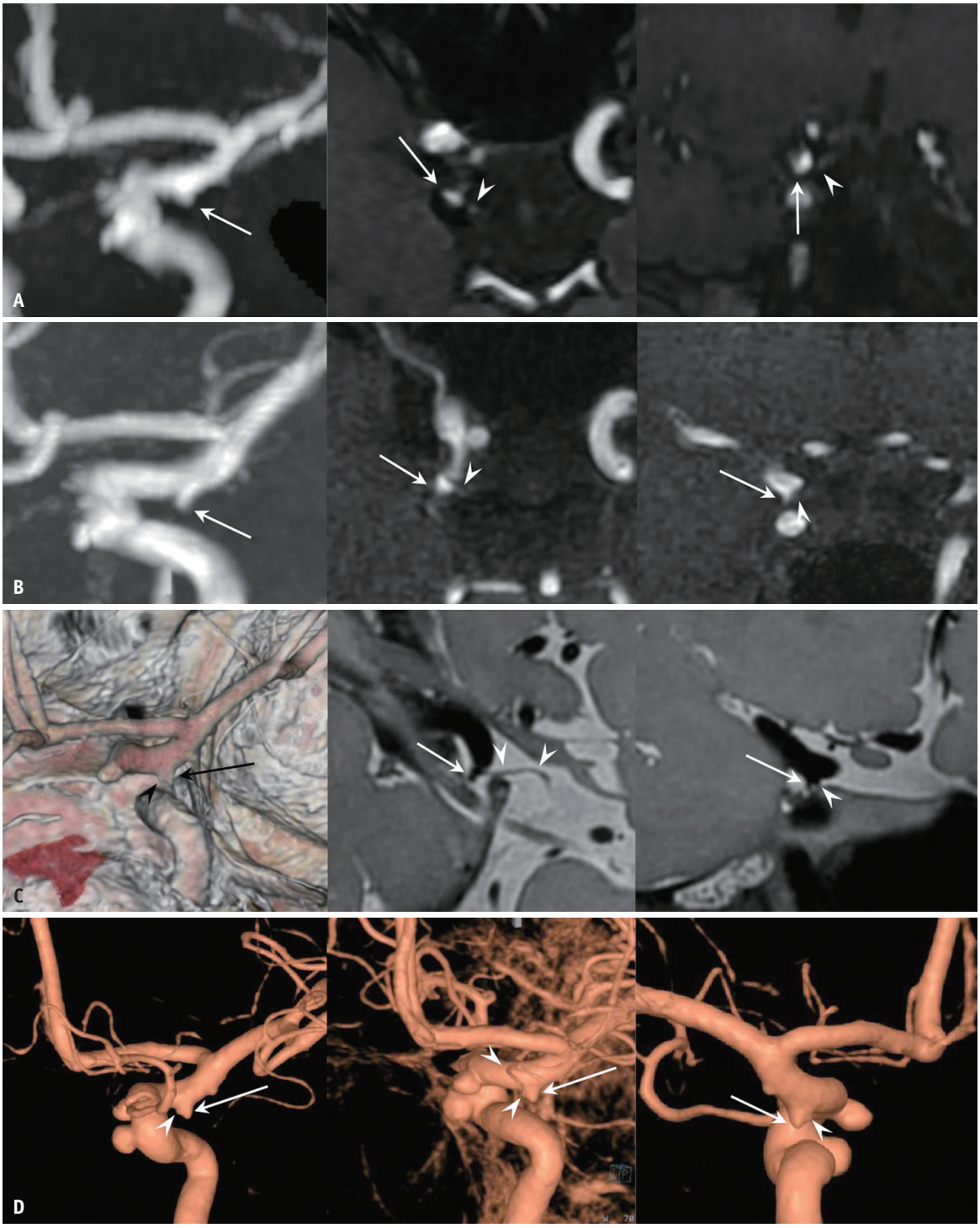

Fig. 3. True-positive case in a 47-year-old female patient that was correctly identified on PD-MRA. **A:** An indeterminate lesion is depicted at the origin of the right Pcom (arrow) on a MIP image of conventional MRA (left). The relationship between the indeterminate lesion (arrows) and Pcom (arrowheads) is not apparent on axial (middle) and coronal MPR images (right). **B:** An indeterminate lesion (arrow) is depicted on a VR image of HR-MRA (left). A faint linear branching vessel (arrowheads) is suspected on a sagittal MPR image (middle, right), but the relationship with the indeterminate lesion (arrows) is not obvious. One reader diagnosed it as an aneurysm. **C:** A VR image of PD-MRA shows an indeterminate lesion (arrow) and another tiny vascular bulging structure (arrowhead) (left). MPR images clearly show the indeterminate lesion (arrows), laterally protruding from the origin of the Pcom (arrowheads) in different directions (middle, right). All readers diagnosed it as an aneurysm. **D:** Three-dimensional rotational angiography images confirmed the aneurysm (arrows) at the origin of the right Pcom (arrowheads). PD-MRA = proton-density MR angiography, Pcom = posterior communicating artery, MIP = maximal intensity projection, MPR = multiplanar reconstruction, VR = volume rendering, HR-MRA = high-resolution time-of-flight MR angiography

https://doi.org/10.3348/kjr.2023.1241

Korean Journal of Radiology
KJR

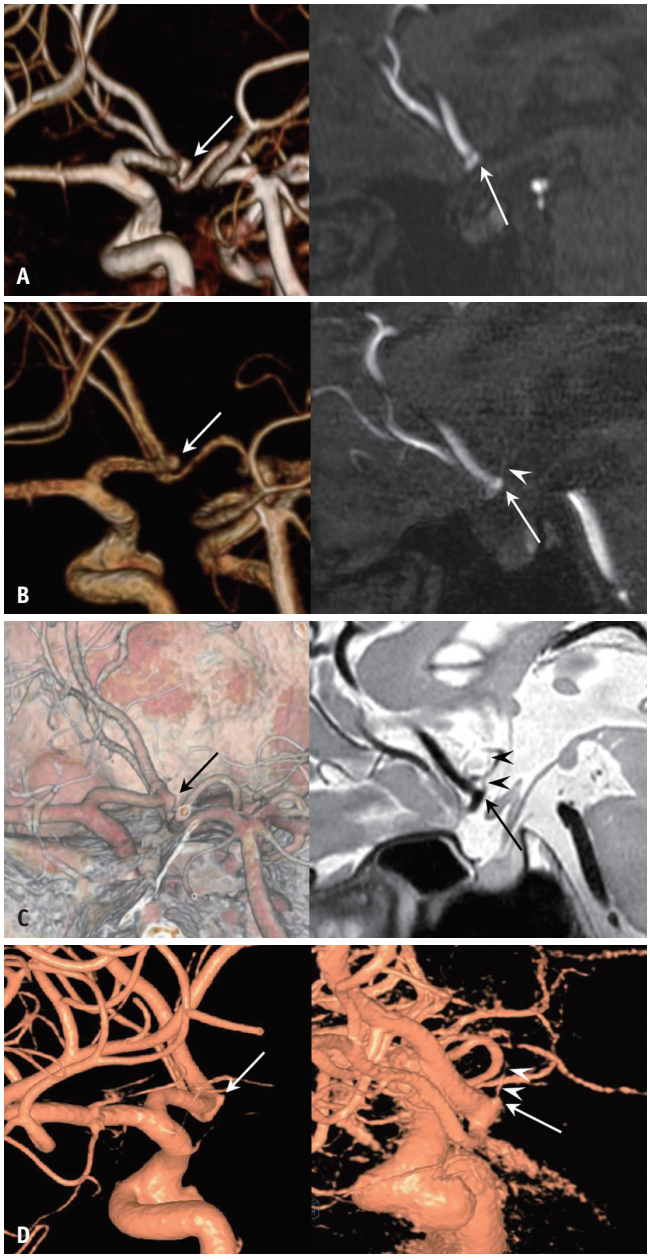

Fig. 4. True-negative case in a 55-year-old male patient that was correctly identified on PD-MRA. **A:** An indeterminate lesion (arrows) is depicted in the Acom on VR (left) and sagittal MPR (right) images of conventional MRA. **B:** An indeterminate lesion (arrow) is depicted on a VR image of HR-MRA (left). A faint linear branching vessel (arrowhead) is suspected on a sagittal MPR image (right), but the relationship with the indeterminate lesion (arrow) is not obvious. One reader diagnosed it as an aneurysm. **C:** A VR image of PD-MRA shows an indeterminate lesion (arrow, left), and a branching vessel (arrowheads) originating from the apex of the indeterminate lesion (arrow) is depicted on sagittal MPR image (right). All readers diagnosed it as an infundibulum. **D:** Three-dimensional rotational angiography images confirmed a branching vessel (arrowheads) with infundibulum (arrows). PD-MRA = proton-density MR angiography, Acom = anterior communicating artery, VR = volume rendering, MPR = multiplanar reconstruction, MRA = MR angiography, HR-MRA = high-resolution time-of-flight MR angiography

variations within indeterminate lesions. Additionally, our study highlighted the added value of PD-MRA in both the AND (indicating an aneurysm only if both HR-MRA and PD-MRA results suggest an aneurysm) and OR (indicating an aneurysm if either result suggests an aneurysm) combination algorithms, which showed significantly higher accuracy than using HR-MRA alone. The inter-reader agreement for PD-MRA exceeded that of HR-MRA, suggesting PD-MRA could serve as an important alternative imaging modality before proceeding to DSA and may be preferred over follow-up imaging when conventional CTA or MRA reveal lesions indeterminate for intracranial aneurysms.

To our knowledge, no study has yet explored indeterminate lesions where intracranial aneurysms are suspected and shown a significant diagnostic improvement when comparing PD-MRA with TOF-MRA at the same spatial resolution. The proliferation and advancement of imaging technologies have led to the identification of a considerable number of indeterminate lesions, regardless of whether they are intracranial aneurysms. Recent studies have highlighted the supportive role of deep learning algorithms in CTA and MRA in interpreting aneurysms, showing an increase in sensitivity (87%–92%) and a reduction in reading time [23,24]. However, challenges remain with false-positive detections and difficulties in accurately identifying small aneurysms under 3 mm [25]. Reports indicate that up to 18% of TOF-MRA scans on 3T machines have identified indeterminate lesions, often due to their small size (< 3–5 mm) [6]. Recent studies suggest that small intracranial aneurysms of less than 3 mm pose a relatively high risk of rupture risk [26,27], contradicting the previous belief that smaller aneurysms generally have a low rupture risk [28]. Thus, there is a need to refine conventional imaging methods like CTA or MRA for evaluating small intracranial aneurysms or indeterminate lesions to distinguish aneurysms from normal variations more effectively. HR-MRA, with a spatial resolution of less than 0.3 mm, has been extensively researched using 7T machines, which have been shown to improve inter-reader agreement and provide clearer assessments of aneurysms, enhancing diagnostic certainty over conventional MRA. However, the clinical application of 7T MRI is limited [6,14,18,19]. Similarly, high-resolution CTA, also known as ultra-high-resolution CTA with a spatial resolution of less than 0.2 mm, faces limitations as only a few advanced machines are capable of achieving such performance [29,30]. In our study, PD-MRA demonstrated excellent diagnostic performance for indeterminate lesions, with the majority (97.9%) being less

https://doi.org/10.3348/kjr.2023.1241

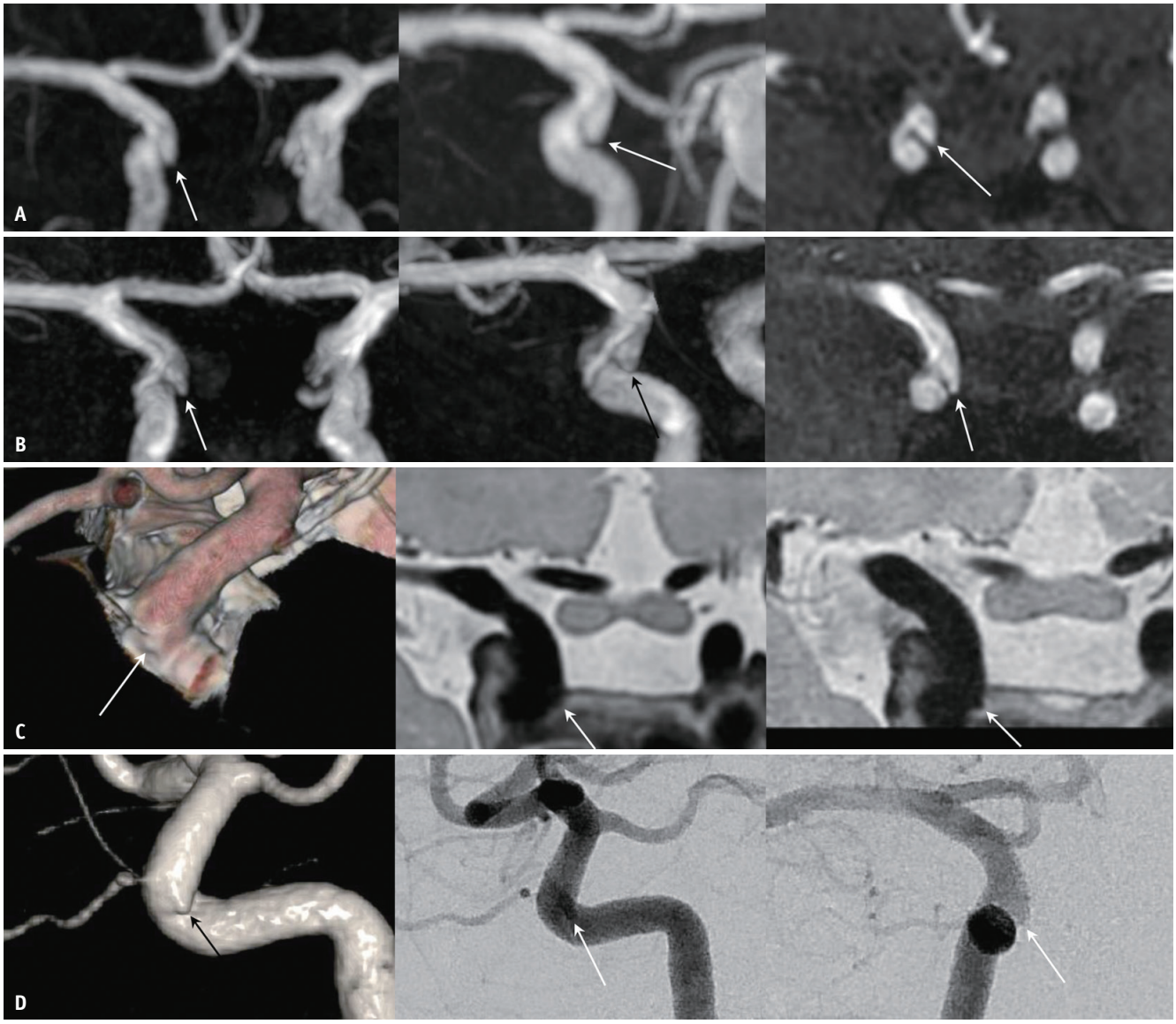

Fig. 5. A false-negative case in a 47-year-old female patient who was misdiagnosed with PD-MRA. **A:** MIP (left, middle) and coronal MPR (right) images of conventional MRA show vascular bulging (arrows) at the right paraclinoid ICA. **B:** MIP (left, middle) and coronal MPR (right) images of HR-MRA show vascular bulging (arrows) more clearly, and all readers diagnosed it as an aneurysm. **C:** VR (left) and coronal MPR (middle) images of 0.25^3-mm^3 PD-MRA showed subtle vascular bulging (arrows) at the right paraclinoid ICA. The lesion is located within the cavernous sinus, and two readers misdiagnosed it. Coronal MPR (right) images of 0.2^3-mm^3 PD-MRA present a better depiction of the right paraclinoid ICA aneurysm than 0.25^3-mm^3 PD-MRA. **D:** Three-dimensional rotational angiography (left) and frontal and lateral DSA (middle, right) images confirmed the aneurysm (arrows) at the right paraclinoid ICA. PD-MRA = proton-density MR angiography, MIP = maximal intensity projection, MPR = multiplanar reconstruction, MRA = MR angiography, ICA = internal carotid artery, HR-MRA = high-resolution time-of-flight MR angiography, VR = volume rendering, DSA = digital subtraction angiography

than 3 mm in size. Given its high availability, superior SNR, and the application of various techniques to shorten scan times—such as compressed sensing and advanced parallel imaging—or to enhance image quality, including commercial artificial intelligence, PD-MRA in 3T machines may offer a viable alternative imaging method.

Kim et al. [21] showed the usefulness of PD-MR in distinguishing aneurysms from infundibula in only the posterior communicating artery with almost perfect inter-observer agreement and a sensitivity of 98.6% and specificity of 45.5%. However, their study was limited to cases originating from the posterior communicating artery and did not address lesion size or indeterminate lesions. Yim et al. [5] underscored the additional value of PD-MR in diagnosing aneurysms within the circle of Willis. Still, the unstandardized parameters between PD-MR and TOF-

https://doi.org/10.3348/kjr.2023.1241

Korean Journal of Radiology
KJR

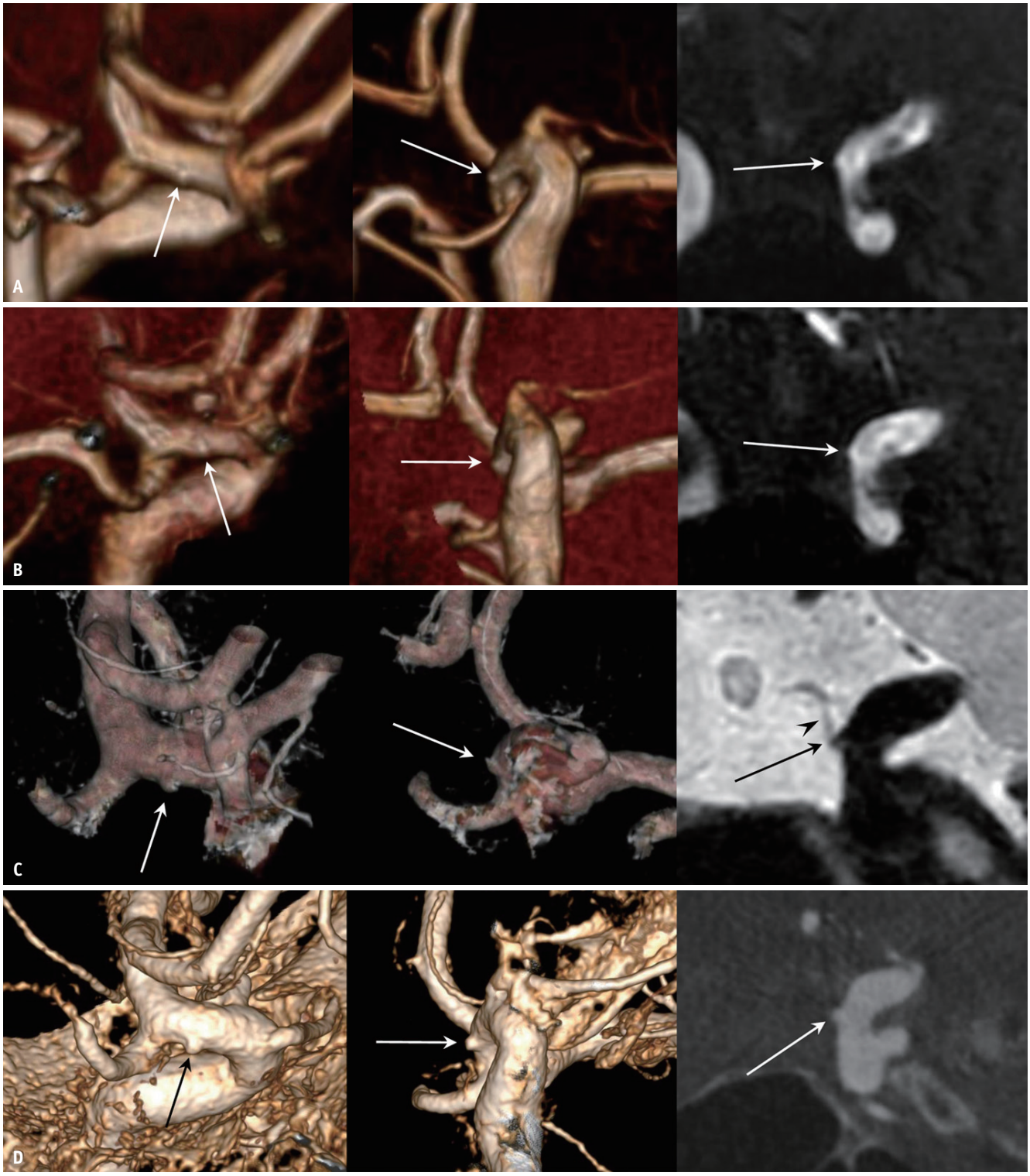

Fig. 6. A false-negative case in a 50-year-old female patient that was categorized as an infundibulum on PD-MRA. **A:** VR (left, middle) and coronal MPR (right) images of conventional MRA show tiny vascular bulging (arrows) at the left paraclinoid ICA. **B:** VR (left, middle) and coronal MPR (right) images of HR-MRA show tiny vascular bulging (arrows) without a branching vessel at the left paraclinoid ICA. All readers diagnosed it as an aneurysm. **C:** VR (left, middle) and coronal MPR (right) images of PD-MRA show cone-shaped vascular bulging (arrows) with a definite branching vessel from the dome (arrowhead). All readers diagnosed it as an infundibulum. **D:** Source image of three-dimensional rotational angiography (right) and its VR images (left, middle) shows vascular bulging (arrows) without a depiction of the branching artery, which resulted in the false-negative. PD-MRA = proton-density MR angiography, VR = volume rendering, MPR = multiplanar reconstruction, MRA = MR angiography, ICA = internal carotid artery, HR-MRA = high-resolution time-of-flight MR angiography

https://doi.org/10.3348/kjr.2023.1241

MRA limited the ability to establish the superiority of PD-MR over TOF-MRA. Moreover, no prior studies have shown the reconstruction of 3D images, such as volume rendering, which could be comparable to CTA or MRA and expand its clinical application. Therefore, in our terminology, we refer to it as PD-MRA rather than PD-MR. Our study highlighted PD-MRA's superior diagnostic performance with reconstructed images in selectively indeterminate lesions of challenging cases in clinical settings, using standardized parameters for PD-MRA and HR-MRA. Additionally, our research found added value in combining PD-MRA with HR-MRA through AND and OR algorithms, achieving higher accuracy than HR-MRA alone, echoing findings from previous research.

Of the seven aneurysms that were concordantly missed in two or more readers (FN), five were located near the cavernous sinus, sphenoid sinus, or clinoid bones, and two lesions were located near the brain parenchyma or tortuous arteries. Therefore, lesions not delineated by CSF spaces require cautious interpretation. The volume rendering capabilities of PD-MRA are limited by the presence of bone and air structures, leading to relatively higher false-negative outcomes in paraclinoid or cavernous ICA lesions.

This study is subject to several limitations. Firstly, it was designed retrospectively, and despite prior sample size calculations, the patient population may still be considered small. Secondly, it focused exclusively on unruptured intracranial aneurysms. Thirdly, 0.2^3-mm^3 HR-MRA was excluded due to its low SNR and extended scan durations, which limit its practical application in clinical settings. Fourthly, 9.2% of the patients did not receive 3D-rotational angiography with volume rendering, potentially affecting the diagnostic accuracy. Fifthly, the volume rendering of PD-MRA was not performed using specialized software but with the AquariusNET viewer from TeraRecon, which restricts the exclusion of sphenoid sinuses and clinoid bones near the distal ICA. Hence, there is a need for further advancements in post-processing techniques.

In conclusion, our study revealed that PD-MRA offers superior diagnostic performance compared to HR-MRA and nearly perfect inter-reader agreement in diagnosing aneurysms among patients with indeterminate lesions on conventional CTA or MRA. As such, PD-MRA may minimize the necessity for invasive diagnostic angiography and avoid the need for unnecessary follow-up imaging.

Supplement

The Supplement is available with this article at https://doi.org/10.3348/kjr.2023.1241.

Availability of Data and Material

The datasets generated or analyzed during the study are available from the corresponding author on reasonable request.

Conflicts of Interest

The authors have no potential conflicts of interest to disclose.

Author Contributions

Conceptualization: Seung Chai Jung. Data curation: Pae Sun Suh, Seung Chai Jung, Keum Mi Choi. Formal analysis: Pae Sun Suh, Seung Chai Jung, Hye Hyeon Moon, Yun Hwa Roh, Yunsun Song. Funding acquisition: Seung Chai Jung. Investigation: Pae Sun Suh, Seung Chai Jung. Methodology: Pae Sun Suh, Seung Chai Jung, Jungbok Lee. Project administration: Seung Chai Jung. Resources: Seung Chai Jung, Yunsun Song. Software: Pae Sun Suh, Seung Chai Jung, Keum Mi Choi. Supervisor: Seung Chai Jung. Validation: Pae Sun Suh, Seung Chai Jung, Jungbok Lee. Visualization: Pae Sun Suh, Seung Chai Jung. Writing—original draft: Pae Sun Suh, Seung Chai Jung, Jungbok Lee. Writing—review & editing: Seung Chai Jung.

ORCID IDs

Pae Sun Suh
https://orcid.org/0000-0002-8618-9558
Seung Chai Jung
https://orcid.org/0000-0001-5559-7973
Hye Hyeon Moon
https://orcid.org/0000-0001-8484-3117
Yun Hwa Roh
https://orcid.org/0000-0002-8041-1621
Yunsun Song
https://orcid.org/0000-0003-4738-0533
Minjae Kim
https://orcid.org/0000-0002-5382-9360
Jungbok Lee
https://orcid.org/0000-0002-1420-9484
Keum Mi Choi
https://orcid.org/0000-0002-6934-8027

Korean Journal of Radiology
KJR

Funding Statement

This study was supported by the National Research Foundation of Korea (NRF) grant funded by the Korea government (NRF-2020M3E5D2A01084578).

REFERENCES

1. Jeon TY, Jeon P, Kim KH. Prevalence of unruptured intracranial aneurysm on MR angiography. *Korean J Radiol* 2011;12:547-553
2. Park S, Lee DH, Ryu CW, Pyun HW, Choi CG, Kim SJ, et al. Incidental saccular aneurysms on head MR angiography: 5 years' experience at a single large-volume center. *J Stroke* 2014;16:189-194
3. Sun LJ, Li YD, Li MH, Wang W, Gu BX. Aneurysm outflow angle at MRA as discriminant for accurate diagnosis and differentiation between small sidewall cerebral aneurysms and infundibula. *J Neurointerv Surg* 2017;9:591-594
4. Yang ZL, Ni QQ, Schoepf UJ, De Cecco CN, Lin H, Duguay TM, et al. Small intracranial aneurysms: diagnostic accuracy of CT angiography. *Radiology* 2017;285:941-952
5. Yim Y, Jung SC, Kim JY, Kim SO, Kim BJ, Lee DH, et al. Added diagnostic values of three-dimensional high-resolution proton density-weighted magnetic resonance imaging for unruptured intracranial aneurysms in the circle-of-Willis: comparison with time-of-flight magnetic resonance angiography. *PLoS One* 2020;15:e0243235
6. Radojewski P, Slotboom J, Joseph A, Wiest R, Mordasini P. Clinical implementation of 7T MRI for the identification of incidental intracranial aneurysms versus anatomic variants. *AJNR Am J Neuroradiol* 2021;42:2172-2174
7. van der Schaaf IC, Brilstra EH, Rinkel GJ, Bossuyt PM, van Gijn J. Quality of life, anxiety, and depression in patients with an untreated intracranial aneurysm or arteriovenous malformation. *Stroke* 2002;33:440-443
8. Juvela S, Poussa K, Porras M. Factors affecting formation and growth of intracranial aneurysms: a long-term follow-up study. *Stroke* 2001;32:485-491
9. Salih M, Salem M, Moore J, Thomas AJ, Ogilvy CS. Cost-effectiveness analysis on small (< 5 mm) unruptured intracranial aneurysm follow-up strategies. *J Neurosurg* 2022;138:1366-1373
10. Kaufmann TJ, Huston J 3rd, Mandrekar JN, Schleck CD, Thielen KR, Kallmes DF. Complications of diagnostic cerebral angiography: evaluation of 19,826 consecutive patients. *Radiology* 2007;243:812-819
11. Chen X, Liu Y, Tong H, Dong Y, Ma D, Xu L, et al. Meta-analysis of computed tomography angiography versus magnetic resonance angiography for intracranial aneurysm. *Medicine (Baltimore)* 2018;97:e10771
12. Zhang X, Cao YZ, Mu XH, Sun Y, Schmidt M, Forman C, et al. Highly accelerated compressed sensing time-of-flight magnetic resonance angiography may be reliable for diagnosing head and neck arterial steno-occlusive disease: a comparative study with digital subtraction angiography. *Eur Radiol* 2020;30:3059-3065
13. Meixner CR, Liebig P, Speier P, Forman C, Hensel B, Schmidt M, et al. High resolution time-of-flight MR-angiography at 7 T exploiting VERSE saturation, compressed sensing and segmentation. *Magn Reson Imaging* 2019;63:193-204
14. Wrede KH, Johst S, Dammann P, Özkan N, Mönninghoff C, Kraemer M, et al. Improved cerebral time-of-flight magnetic resonance angiography at 7 Tesla--feasibility study and preliminary results using optimized venous saturation pulses. *PLoS One* 2014;9:e106697
15. Suzuki T, Natori T, Sasaki M, Miyazawa H, Narumi S, Ito K, et al. Evaluating recanalization of relevant lenticulostriate arteries in acute ischemic stroke using high-resolution MRA at 7T. *Int J Stroke* 2021;16:1039-1046
16. Liu X, Zhang Z, Zhu C, Feng J, Liu P, Kong Q, et al. Wall enhancement of intracranial saccular and fusiform aneurysms may differ in intensity and extension: a pilot study using 7-T high-resolution black-blood MRI. *Eur Radiol* 2020;30:301-307
17. Feng J, Liu X, Zhang Z, Wu Y, Li Z, Zhang Q, et al. Comparison of 7 T and 3 T vessel wall MRI for the evaluation of intracranial aneurysm wall. *Eur Radiol* 2022;32:2384-2392
18. Leemans E, Cornelissen B, Sing MLC, Sprengers M, van den Berg R, Roos Y, et al. 7T versus 3T MR angiography to assess unruptured intracranial aneurysms. *J Neuroimaging* 2020;30:779-785
19. Radojewski P, Dobrocky T, Branca M, Almiri W, Correia M, Raabe A, et al. Diagnosis of small unruptured intracranial aneurysms: comparison of 7 T versus 3 T MRI. *Clin Neuroradiol* 2024;34:45-49
20. Lee SH, Jung SC, Kang DW, Kwon SU, Kim JS. Visualization of culprit perforators in anterolateral pontine infarction: high-resolution magnetic resonance imaging study. *Eur Neurol* 2017;78:229-233
21. Kim S, Chung J, Cha J, Kim BM, Kim DJ, Kim YB, et al. Usefulness of high-resolution three-dimensional proton density-weighted turbo spin-echo MRI in distinguishing a junctional dilatation from an intracranial aneurysm of the posterior communicating artery: a pilot study. *J Neurointerv Surg* 2020;12:315-319
22. Landis JR, Koch GG. The measurement of observer agreement for categorical data. *Biometrics* 1977;33:159-174
23. Bizjak Ž, Špiclin Ž. A systematic review of deep-learning methods for intracranial aneurysm detection in CT angiography. *Biomedicines* 2023;11:2921
24. Gu F, Wu X, Wu W, Wang Z, Yang X, Chen Z, et al. Performance of deep learning in the detection of intracranial aneurysm: a systematic review and meta-analysis. *Eur J Radiol* 2022;155:110457
25. Kallmes DF, Erickson BJ. Automated aneurysm detection: emerging from the shallow end of the deep learning pool. *Radiology* 2021;298:164-165
26. Ikegami M, Kamide T, Ooigawa H, Take Y, Teranishi A, Suzuki K, et al. Clinical features of ruptured very small intracranial

aneurysms (<3 mm) in patients with subarachnoid hemorrhage. *World Neurosurg* 2022;164:e1087-e1093
27. Park GT, Kim JH, Jung YJ, Chang CH. Characteristics of patients with ruptured very small intracranial aneurysm sized less than 3 mm. *J Cerebrovasc Endovasc Neurosurg* 2021;23:1-5
28. Wiebers DO, Whisnant JP, Huston J 3rd, Meissner I, Brown RD Jr, Piepgras DG, et al. Unruptured intracranial aneurysms: natural history, clinical outcome, and risks of surgical and endovascular treatment. *Lancet* 2003;362:103-110
29. Meijer FJA, Schuijf JD, de Vries J, Boogaarts HD, van der Woude WJ, Prokop M. Ultra-high-resolution subtraction CT angiography in the follow-up of treated intracranial aneurysms. *Insights Imaging* 2019;10:2
30. Matsushige T, Hashimoto Y, Ogawa T, Makimoto G, Yoshiyama M, Hara T, et al. The impact of high-resolution cone-beam CT findings on decision-making for the treatment of unruptured middle cerebral artery aneurysms. *Neurosurg Rev* 2022;46:26

https://doi.org/10.3348/kjr.2023.1241